

2012

Cavitation Study of a Microhydro Turbine

Jacob Daniel Riglin
Lehigh University

Follow this and additional works at: <http://preserve.lehigh.edu/etd>

Recommended Citation

Riglin, Jacob Daniel, "Cavitation Study of a Microhydro Turbine" (2012). *Theses and Dissertations*. Paper 1134.

This Thesis is brought to you for free and open access by Lehigh Preserve. It has been accepted for inclusion in Theses and Dissertations by an authorized administrator of Lehigh Preserve. For more information, please contact preserve@lehigh.edu.

Cavitation Study for a Microhydro Turbine

by

Jacob Riglin

A Thesis

Presented to the Graduate and Research Committee

of Lehigh University

in Candidacy for the Degree of

Master of Science

in

Mechanical Engineering

Lehigh University

November 10, 2012

This thesis is accepted and approved in partial fulfillment of the requirements for the Master of Science in Mechanical Engineering.

Date Approved

Dr. Alparslan Oztekin

Advisor

Dr. D. Gary Harlow

Department Chair Person

Table of Contents

List of Figures.....	i
List of Tables.....	iii
Abstract.....	1
Introduction.....	2
Thesis Statement.....	9
Mathematical Modeling & Numerical Methods.....	10
Results and Discussion	23
Conclusions.....	34
References	36
Appendices.....	38
Vita.....	48

List of Figures

Figure 1. Gap induced cavitation for a flow of .353 m ³ /s and a rotation rate of 1150 rpm [10].	4
Figure 2. Cavitation sheets produced along blades for flow conditions of (a) 0.314 m ³ /s and (b) 0.353 m ³ /s [10].	5
Figure 3. Uniform blade geometry.	5
Figure 4. 1.5 Pitch, non-uniform blade geometry.	6
Figure 5. Plots of Head (a), Power (b,c) and Efficiency (d) as a function of flow rate for the 1.5 pitch geometry [17].	7
Figure 6. Pressure contour along the blade of 1.5 pitch geometry for a flow rate of .1m ³ /s and a rotation rate of 750 rpm [17].	8
Figure 7. Cross sectional view of blade meshing.	11
Figure 8. Exit fluid domain meshing (left) and additional meshing layers along the housing and blade (right).	11
Figure 9. Velocity distribution at the inlet for flow rate of 0.1 m ³ /s.	16
Figure 10. Flow chart for transient simulations [20].	19
Figure 11. Secondary volume produced for Cavitation number study.	22
Figure 12. Pressure contour with vortex core region based on a swirl intensity of 676.3 s ⁻¹ for multiphase flow (above) and single phase flow (below) at a flow rate of .1 m ³ /s and a rotation rate of 500 rpm.	24
Figure 13. Vapor fraction along blade on 1.5 pitch geometry with flow rate of 0.0625 m ³ /s and a rotation rate of 500 rpm.	26
Figure 14. Vapor fraction along blade on uniform geometry with flow rate of 0.5 m ³ /s and a rotation rate of 500 rpm.	26
Figure 15. Cavitation on blade of 1.5 pitch geometry operating at a rotation rate of 500 rpm for flow rates of 0.0625 m ³ /s (top left), 0.075 m ³ /s (top right), 0.0875 m ³ /s (bottom left), and 0.1 m ³ /s (bottom right).	27
Figure 16. Volume fraction exiting the turbine for the 1.5 pitch geometry at a flow of 0.1 m ³ /s and a rotation rate of 500 rpm.	28
Figure 17. Head as a function of flow rate for multiphase and single phase models simulations with the 1.5 pitch geometry and rotation rate of 500 rpm.	29

Figure 18. Power as a function of flow rate for multiphase and single phase simulations with the 1.5 pitch geometry and rotation rate of 500 rpm. 29

Figure 19. Efficiency as a function of flow rate for both multiphase and single phase simulations with the 1.5 pitch geometry and rotation rate of 500 rpm. 30

Figure 20. Cavitation number (left) and volume fraction (right) contours along the blade for the multiphase simulation with flow rate of 0.1 m³/s..... 32

Figure 21. Cavitation number along blade for single phase simulation with flow rate of 0.1 m³/s..... 32

Figure 22. Cavitation number (left) and volume fraction (right) contours along the blade for the multiphase simulation with flow rate of 0.0625 m³/s..... 33

Figure 23. Cavitation number along blade for single phase simulation with flow rate of 0.0625 m³/s..... 33

List of Tables

Table E1. Data for 1.5 pitch geometry, rotation rate of 500 rpm, multiphase	47
Table E2. Data for 1.5 pitch geometry, rotation rate of 500 rpm, single phase	47
Table E3. Data for uniform geometry, rotation rate of 500 rpm.....	47

Abstract

Cavitation produces undesirable effects within turbines, such as noise, decreases in efficiency, and structural degradation of the device. The cavitation effects existing within two microhydro turbines with two different blade geometries, 1.5 pitch and uniform pitch, were determined with the aid of FLUENT, a CFD-based software package. A method was produced that could be used to determine where cavitation occurs along the blade and within the flow for various inlet flow rates. To reduce the rigidity of the problem, "SIMPLEC" was used as the solution control with "PRESTO!" being used to correct the pressure between iterations. Cavitation number was used to correlate the single phase to the multiphase results, allowing for the single phase simulations to be used to determine where the onset of cavitation occurs. It was determined that cavitation occurred at the exit of the blade between a flow rate of 0.05 m³/s and .0625 m³/s for the 1.5 pitch geometry and 0.25 m³/s and 0.5 m³/s for the uniform geometry. As the flow rate exceeded the point where the onset of cavitation occurs, the intensity of cavitation increases and efficiency drops of up to 12% were experienced by the turbines. With the use of the Cavitation number, it was determined that the critical Cavitation number where the onset of cavitation occurs is approximately -10,000 to -20,000. Additionally, the Cavitation number contours for the single phase and multiphase simulation are similar enough to allow for the single phase simulation to be used in determining the onset of cavitation, thus decreasing the computational time and resources needed to determine where and when cavitation occurs.

Introduction

Micro-hydropower utilizes energy existing in flowing water to produce electricity, through the use of a generator, or mechanical energy. Micro-hydro systems are typically utilized in mountainous regions that have naturally occurring head due to the elevation change or in streams or rivers that have high free stream velocities at the surface. Micro-hydro systems typically utilize a turbine or pump to transform the energy within the flow, delivered with the use of a penstock, to some other form, typically electricity [1]. Throughout the United States, the availability of micro-hydropower can be determined geographically utilizing Virtual Hydropower Prospector [2].

Small hydro is an excellent power source for developing countries and remote locations. Micro-hydro installations have been proven to be an excellent, cost-effective choice for power production in remote villages in India [3]. These systems offer the possibility of a run-of-the-river intake where a penstock diverts flow from a stream to pass through the turbine without the need for construction of a dam. While there is no international agreement on the range of power classification, micro hydro typically involves a hydro power station that produces less than 500 kW of power [4].

Studies have been done testing radial and mixed flow turbines that operate at low heads, producing more than 70% efficiency, to optimize the design of blades, inlet, and outlet regions [5] [6] [7] [8]. More specifically, the penstocks leading into low-head, micro-hydro systems were optimized, yielding the appropriate inlet

diameter for given penstocks. Blades have been optimized in a way to produce micro-hydro turbines that encompass a wide range of heads and outputs. By using key dimensions for a reference model and scaling individual blades, axial turbine models may be designed for specific locations and achieve additional benefits, such as limiting manufacturing difficulties and debris blockage resistance [5] [8] [9].

Cavitation is an undesirable effect that results within flow due to the local pressure within the fluid dropping to some point below the vaporization pressure of the fluid. Cavitation specifically deals with the vaporization of the fluid at regions where boiling occurs as the pressure is sufficiently low. Bubbles that form at some point become unstable and collapse within the flow. The instabilities that occur due to bubble formation and destruction can result in negative effects such as noise and structural damage any component near bubble inception. Therefore, it is desirable to test for cavitation, especially within devices such as turbomachinery.

Computational fluid dynamic analyses have been conducted on a wide array of turbine designs, allowing for the performance properties to be obtained. Cavitation along the blades of a Kaplan turbine was determined to occur on the outer most, trailing edge [10]. Advancements have been made in the modeling of cavitation using CFD software, such as Fluent [11]. The Cavitation-Induced-Momentum-Defect (CIMD) approach accounts for both cavitation inception and collapse occurrences within the momentum model of the liquid phase. In addition, homogeneous equilibrium model assumptions are applied and compressibility effects are accounted for [12]. CIMD allows for the modeling of cavitation induced

turbulence resulting in chaotic flows, which allow it to be applied to the modeling of pumps and turbines. Computational fluid dynamic analyses allow properties within the flow to be determined, but, equally important, visual representations of the flow characteristics can be produced including, streamlines, contours of properties (such as pressure, volume fraction, and shear stress), and nodal properties within the fluid region. Figure 1 shows the cavitation contour along the blade surface of a Kaplan turbine. Regions highlighted in magenta correspond to areas where the void fraction of the vapor phase exceeds 50% and blue regions correspond to vapor fractions that are approximately 0%. Figure 2 shows the cavitating flow at the exit of the turbine that corresponds with Figure 1. Additional studies show characteristics of turbomachinery in conditions where the vapor phase is taken into consideration during transient operation [10] [13] [14] [15]. Results from multiphase simulations are often compared to results obtained from studies detailing experimental results showing both cavitation and the damaged produced from cavitation [16].

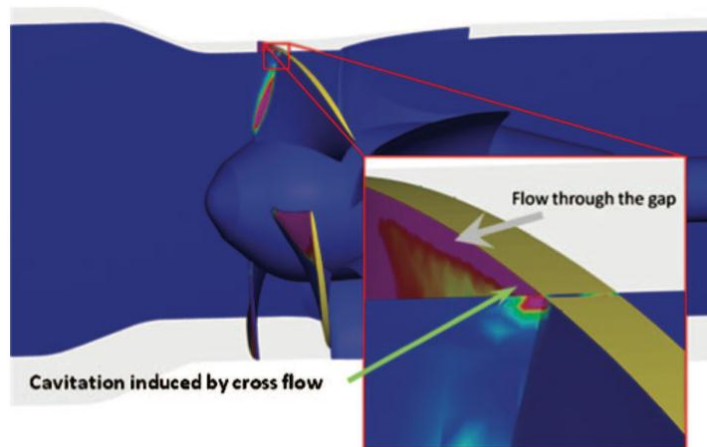


Figure 1. Gap induced cavitation for a flow of $.353 \text{ m}^3/\text{s}$ and a rotation rate of 1150 rpm [10].

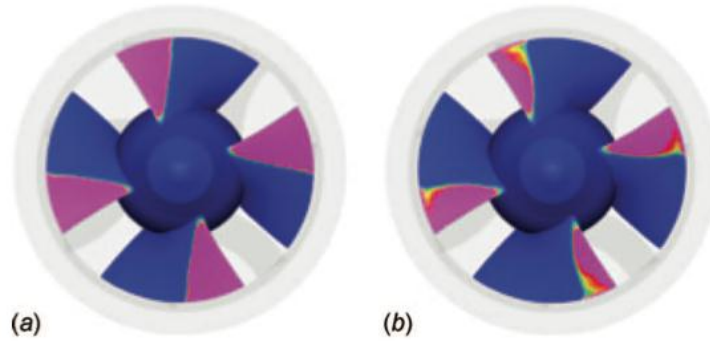


Figure 2. Cavitation sheets produced along blades for flow conditions of (a) $0.314 \text{ m}^3/\text{s}$ and (b) $0.353 \text{ m}^3/\text{s}$ [10].

Axial flow turbines are of great interest, more specifically Archimedes screw designs that can be utilized for flows that have low flow rate and low head. Figure 3 and Figure 4 show basic Archimedes screw blades with the first showing a uniform pitch geometry and the second showing a 1.5 power pitch geometry (dimensioned drawings of both uniform and 1.5 pitch geometries can be seen in Appendix A and Appendix B). Both designs have the same number of turns, consist of the same material, and have the same basic dimensions for blade thickness, shaft diameter, and shaft length. As blade pitch is increased toward the exit, the turbine generates more power at the same head. Efficiency can therefore be improved greatly by increasing the pitch of the blades [17].

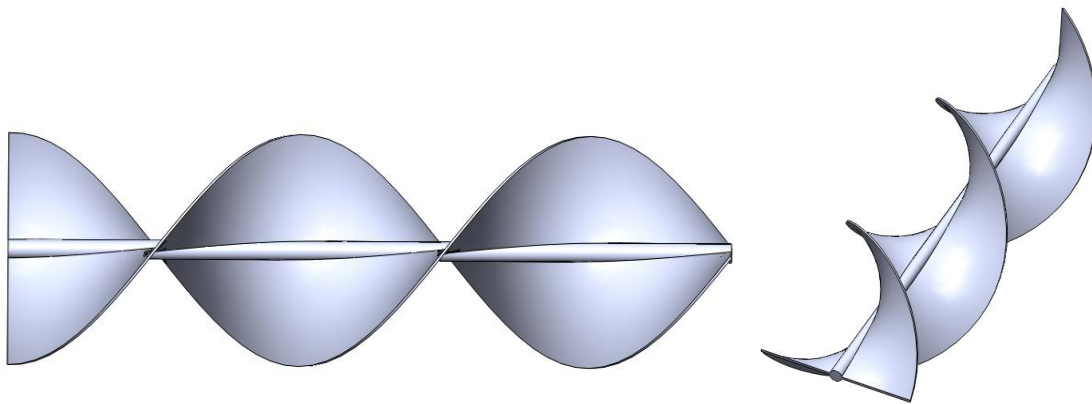


Figure 3. Uniform blade geometry.

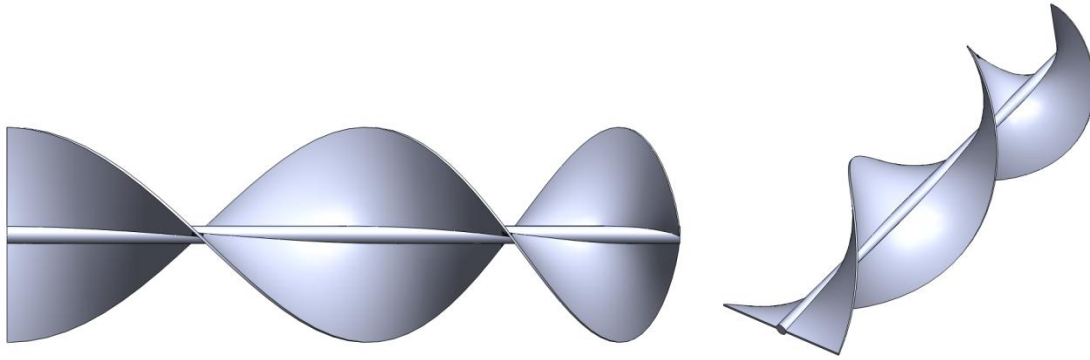


Figure 4. 1.5 Pitch, non-uniform blade geometry.

Figure 5 shows the turbine performance characteristics for the 1.5 pitch geometry based on rotational rates ranging from 200 rpm to 1500 rpm. As seen in Figure 5b and Figure 5c, the power increases much more rapidly as the rotation rate of the blade increases. The maximum efficiency based on the head within the turbine, shown in Figure 5d, is approximately 72%. The critical flow rate at which the maximum efficiency occurs changes based on the rotation rate of the blade. The critical flow rate for 500 rpm is approximately 0.05 m³/s. Figure 6 shows the pressure contours along the blade of the 1.5 pitch geometry during operation at a flow rate of 0.1 m³/s and a rotation rate of 750 rpm. At the exit of the turbine, for geometries involving an increasing blade pitch, a large pressure drop within the flow exists. The blue regions along the blade show the sufficiently low pressures.

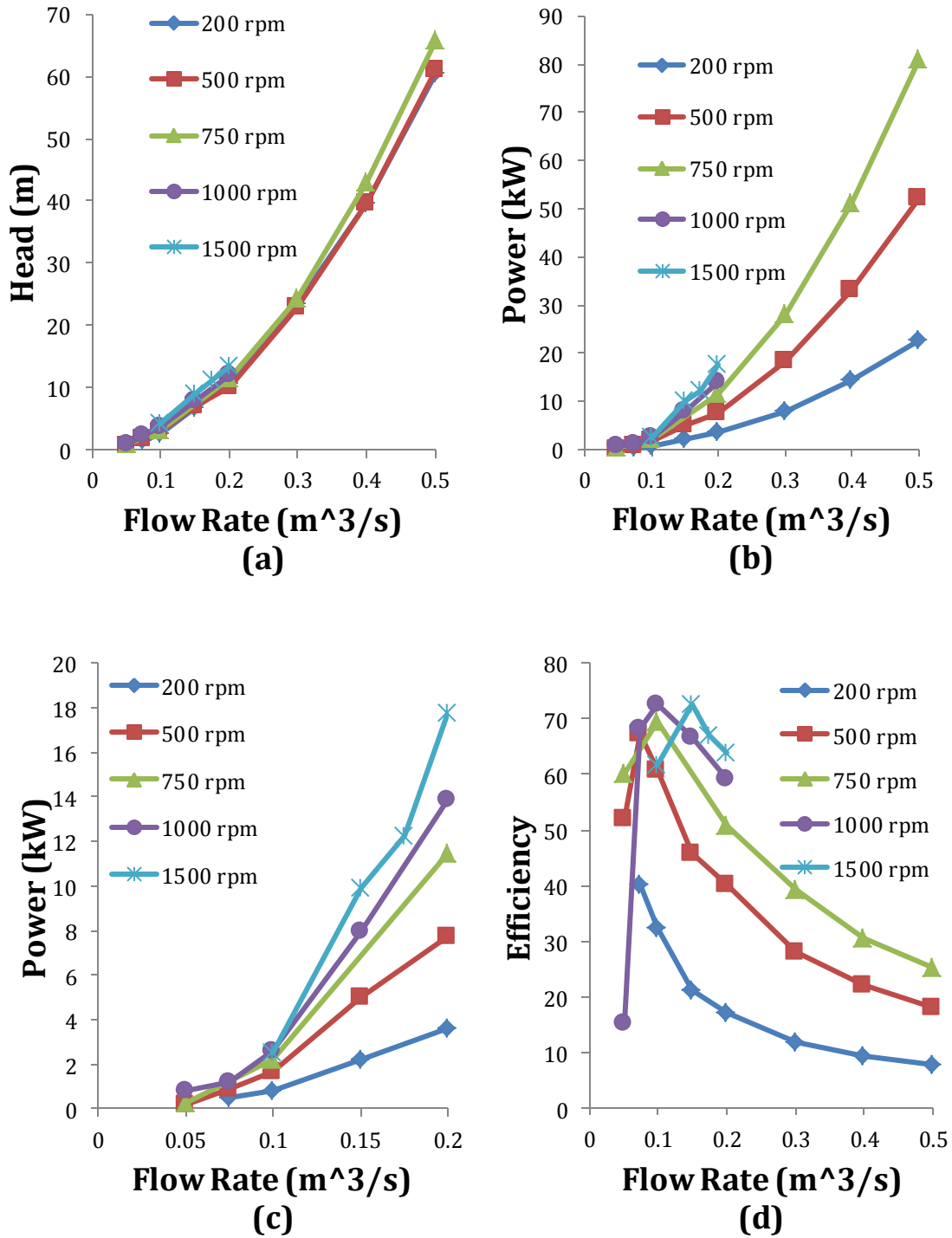


Figure 5. Plots of Head (a), Power (b,c) and Efficiency (d) as a function of flow rate for the 1.5 pitch geometry [17].

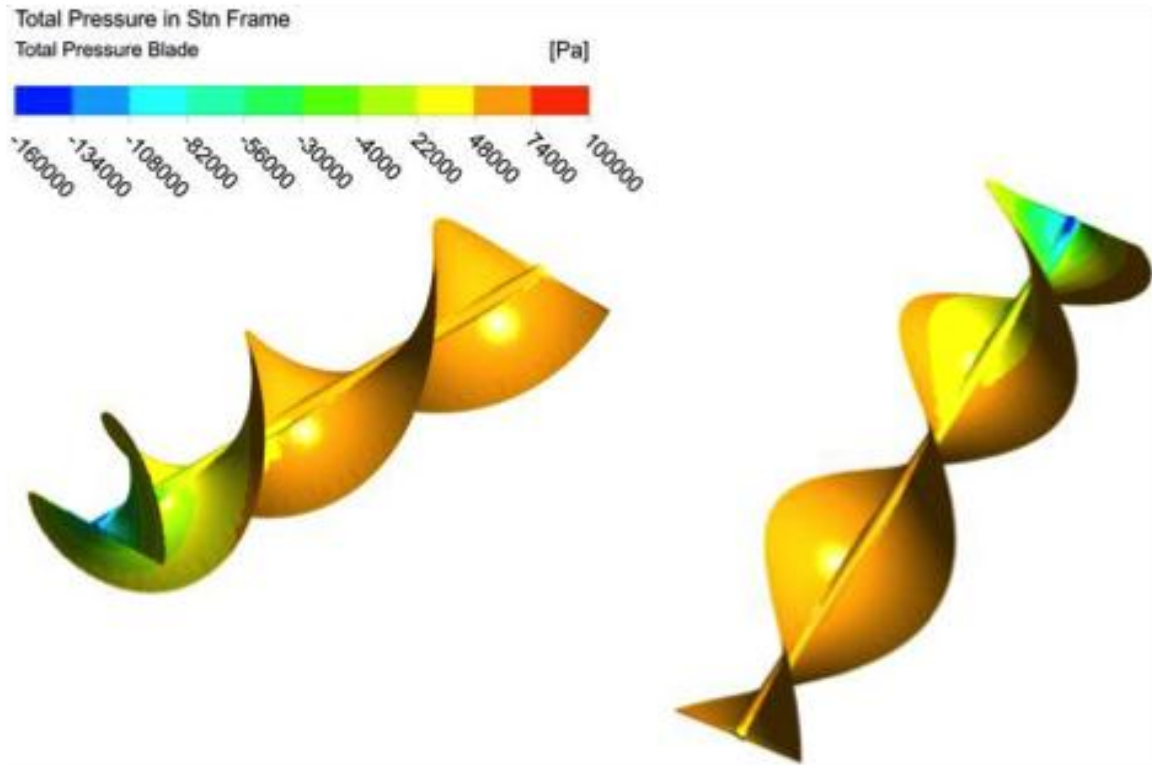


Figure 6. Pressure contour along the blade of 1.5 pitch geometry for a flow rate of .1m³/s and a rotation rate of 750 rpm [17].

Thesis Statement

The primary objective of creating the cavitation model is to produce performance characteristics of the turbine that may be compared directly to the single phase solutions. First and foremost, the cavitation model is to be validated to ensure that results obtained are reasonable. It is necessary to know the onset of cavitation, or the approximate point where cavitation begins to occur. Identifying this value and correlating it to the optimum performance characteristics of the turbine (determined from the single phase solutions) will determine if the onset occurs after the peak efficiency of the turbine. If the critical value of the flow rate for the onset of cavitation is in the range of flow rates yielding the maximum efficiency, the geometry, or the design altogether, may need to be altered. Two main geometries used includes a uniform, 2.5 turn Archimedes screw design and a 1.5 power pitch, 2.5 turn Archimedes screw design. The differences in the onset of cavitation and the cavitation characteristics between both geometries are to be determined in order to identify the effect geometry of the Archimedes screw on cavitation. Finally, a method to compare the single phase flow model to the multiphase flow model using Cavitation number is desirable. Such a method would allow for single phase solutions to be used directly in determining the regions where the volume fraction of the secondary phase becomes relevant.

Mathematical Modeling & Numerical Methods

The 1.5 power pitch geometry was produced using Equation 1 through Equation 4. The x, y, and z-coordinates of the blade were produced in MATLAB. The points were then imported into a CAD software package to produce a 3-D model.

$$t_0 = l_{shaft} \frac{N\pi}{L} \quad (1)$$

Where:

t_0 is a parametric value,

l_{shaft} is the given position along the shaft,

N is the number of blade rotations, and

L is the total shaft length, 0.4953 m.

$$X = R \cos(t_0) \quad (2)$$

Where:

X is the position along the x-axis, and

R is the radius.

$$Y = R \sin(t_0) \quad (3)$$

Where:

Y is the position along the y-axis.

$$Z = L \left(1 - \left(\frac{t_0}{N\pi} \right)^m \right) \quad (4)$$

Where:

Z is the position along the z-axis, and

m is a constant of 1.5.

The meshing utility was used to generate a mesh containing 6083880 elements and 2264377 nodes. Three million nodes provide acceptable results with the current geometry for the single-phase model; however, with the addition of a

second phase a finer mesh was necessary to ensure that the solution would be obtainable and accurate [17]. The mesh, which can be seen in Figure 7 and Figure 8, were used for each simulation conducted. Additional layers of elements were applied to the regions that involve solid to fluid interaction, as well as areas involving highly turbulent activity, to increase the accuracy of the final results.

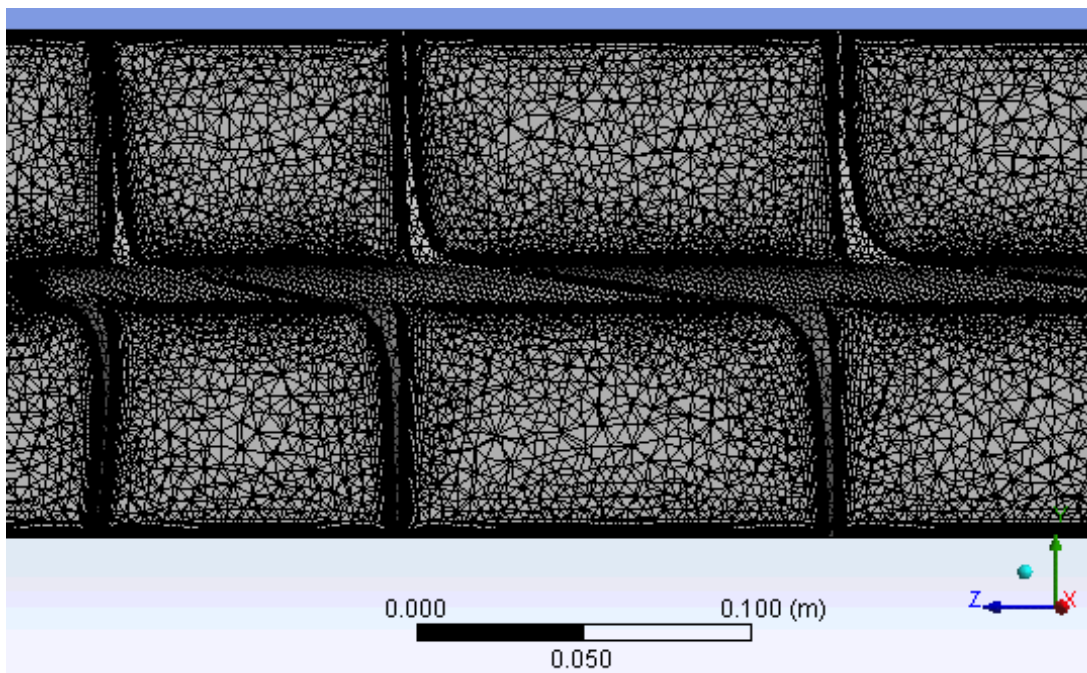


Figure 7. Cross sectional view of blade meshing.

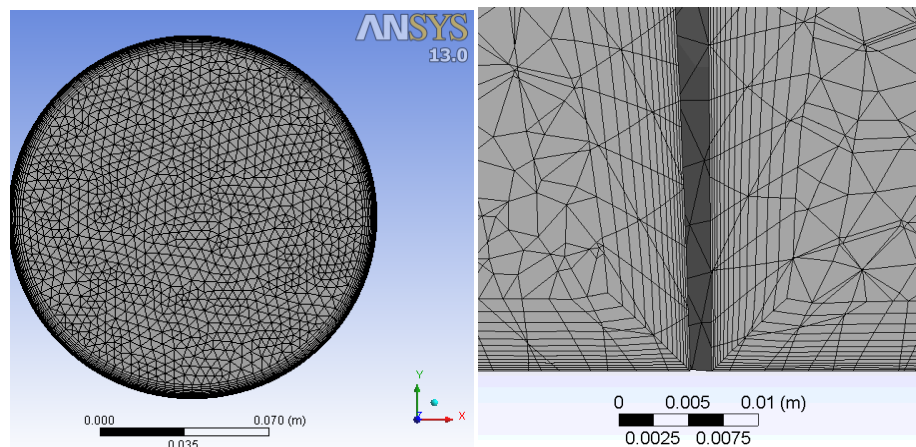


Figure 8. Exit fluid domain meshing (left) and additional meshing layers along the housing and blade (right).

Analyzing the y-plus values along existing solid-fluid interfaces assessed the mesh quality. The y-plus value is a non-dimensional value that is generated from the wall distance that is used in calculating flow profiles over a solid surface. Ideally, y-plus values are less than 200. The mesh that was used provided acceptable y-plus values at even extreme flow rates.

Once the geometries of the uniform pitch blade and the 1.5 power pitch blade were produced using the 3-D modeling, CAD package, the ANSYS meshing utility, FLUENT, and CFD-Post were then used. Once the mesh was generated in the meshing utility, the mesh itself was exported to ensure that the same mesh was used in each simulation and to expedite the setup process for future simulations. Once boundary conditions were applied and the solution converged, CFD-Post was used to analyze the resulting flow characteristics.

Values of Reynolds number occurring from operating flow rates indicated that flow was fully turbulent. The k-epsilon model was used to simulate the turbulence model. More specifically, the renormalized group (RNG) k-epsilon model, developed by [18], was used to offer improvements in modeling turbulence for flow rates resulting in large Reynolds numbers. The RNG k-epsilon model removes the smallest scales of turbulence, allowing for computation to be more feasible and efficient [19]. The transport equations that are used in the RNG k-epsilon method are shown below in Equations 5 through 10:

$$\frac{\partial}{\partial t}(\rho k) + \frac{\partial}{\partial x_i}(\rho k u_i) = \frac{\partial}{\partial x_j} \left[\left(\mu + \frac{\mu_t}{\sigma_k} \right) \frac{\partial k}{\partial x_j} \right] + P_k - \rho \varepsilon \quad (5)$$

Where:

ρ is the density,

μ is the local dynamic viscosity,

μ_t is the turbulent viscosity,

k is the turbulent kinetic energy,

P_k is a product of the turbulent kinetic energy, and

ε is the turbulent dissipation.

$$\frac{\partial}{\partial t}(\rho\varepsilon) + \frac{\partial}{\partial x_i}(\rho\varepsilon u_i) = \frac{\partial}{\partial x_j} \left[\left(\mu + \frac{\mu_t}{\sigma_\varepsilon} \right) \frac{\partial \varepsilon}{\partial x_j} \right] + C_{1\varepsilon} \frac{\varepsilon}{k} P_k - C_{2\varepsilon}^* \rho \frac{\varepsilon^2}{k} \quad (6)$$

Where:

$C_{1\varepsilon}$ is a constant of 1.42, and

$C_{2\varepsilon}^*$ is a constant.

$$C_{2\varepsilon}^* = C_{2\varepsilon} + \frac{C_\mu \eta^3 \left(1 - \frac{\eta}{\eta_0} \right)}{1 + \beta \eta^3} \quad (7)$$

Where:

$C_{2\varepsilon} C_\mu$ is a constant of 1.68,

η is a constant,

η_0 is a constant of 4.8, and

β is a constant of 0.012.

$$\mu_t = \rho C_\mu \frac{k^2}{\varepsilon} \quad (8)$$

Where:

C_μ is a constant of 0.0845.

$$\eta = S \frac{k}{\varepsilon} \quad (9)$$

Where:

S is the modulus of the mean rate-of-strain tensor.

$$S = \left(\sum_i S_i \right)^2 \quad (10)$$

Where:

S_{ij} is rate-of-strain tensor.

The Mixture model was used to simulate the multiphase flow, using liquid water as the primary phase and water vapor as the second phase. The interaction between each phase was set to “cavitation”. Slip velocity between the two phases was neglected. Mixture model continuity equation, momentum equation, and equation for secondary phases can be seen below [20]:

$$\frac{\partial}{\partial t} (\rho_m) + \nabla \cdot (\rho_m \vec{v}_m) \quad (11)$$

Where:

ρ_m is the density of the mixture, and

\vec{v}_m is the mass-averaged velocity.

$$\vec{v}_m = \frac{\sum_{i=0}^n \alpha_m \rho_m \vec{v}_m}{\rho_m} \quad (12)$$

Where:

α is the volume fraction.

$$\rho_m = \sum_{k=1}^n \alpha_k \rho_k \quad (13)$$

$$\frac{\partial}{\partial t} (\rho_m \vec{v}_m) + \nabla \cdot (\rho_m \vec{v}_m \vec{v}_m) = -\nabla P + \nabla \cdot [\mu_m (\nabla \vec{v}_m + \nabla \vec{v}_m^T)] + \quad (14)$$

$$\rho_m \vec{g} + \vec{F} + \nabla \cdot \left(\sum_{k=1}^n \alpha_k \rho_k \vec{v}_{dr,k} \vec{v}_{dr,k} \right)$$

Where:

$\vec{v}_{dr,k}$ is the relative drift velocity, and

μ_m is the viscosity of the mixture.

$$\mu_m = \sum_{k=1}^n \alpha_k \mu_k \quad (15)$$

$$\frac{\partial}{\partial t} (\alpha_p \rho_p) + \nabla \cdot (\alpha_p \rho_p \vec{v}_m) = -\nabla \cdot (\alpha_p \rho_p \vec{v}_{dr,p}) + \sum_{j=1}^n (\dot{m}_{ji} - \dot{m}_{ij}) \quad (16)$$

Where:

\dot{m}_{ij} is the relative mass flow from phase j to phase i.

A fully developed velocity profile was assumed at the computational domain inlet. Equations 17 and 18 show the equations used to produce the velocity distribution at the inlet. An example of the cross-sectional velocity distribution can be seen in Figure 9 shown below.

$$\frac{\bar{u}}{U} = \left(1 - \frac{r}{R}\right)^{1/n} \quad (17)$$

Where:

\bar{u} is the average local velocity,

U is the centerline velocity (maximum velocity),

r is the local radius,

R is the radius at the housing,

n is a constant.

$$n = -1.7 + 1.8 \ln \text{Re}_U \quad (18)$$

Where:

Re_U is the Reynolds number of the pipe flow.

Parameters for the turbulence model were specified through turbulent intensity and length scale. The length scale used was based on the hydraulic diameter [21]. Equation 19 and Equation 20 show the method that was used to

determine the kinetic energy and the turbulent dissipation rate (where $l=0.07D_H$).
Turbulent intensity and hydraulic diameter were set to values of 10% and 0.1524.

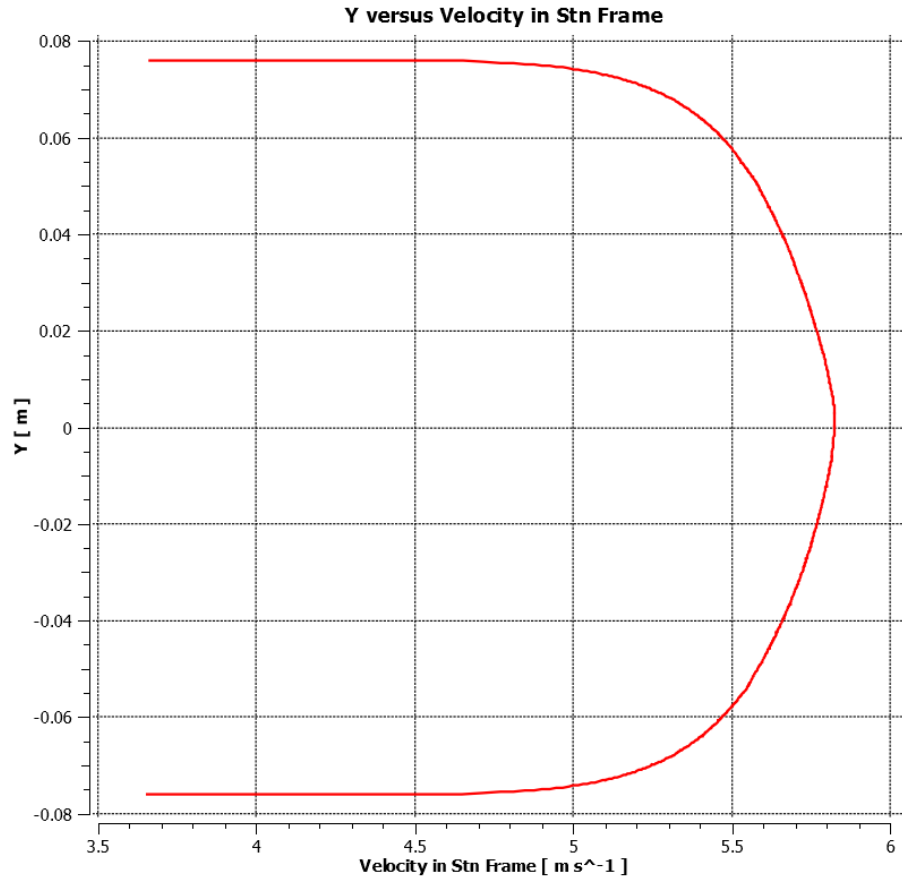


Figure 9. Velocity distribution at the inlet for flow rate of 0.1 m³/s.

$$k = \frac{3}{2} (u_{avg} I_g)^2 \quad (19)$$

Where:

u_{avg} is the average velocity, and

I is the turbulent intensity.

$$\varepsilon = C_\mu^{3/4} \frac{k^{3/2}}{l} \quad (20)$$

Where:

l is the characteristic length.

At the inlet, the velocity was set to a given value using a file that utilized Equations 17 and 18. The pressure at the outlet was set to zero Pascals. The blade was held stationary by assigning a rotation rate of zero radians per second while the frame motion was set to 52.36 radians per second. The stationary wall option was selected for the wall of the fluid. The no-slip condition was applied to both the wall of the fluid and the blade. With the addition of a second phase, two additional boundary conditions were needed for the inlet and the outlet. The vapor phase volume fraction was assigned to values of zero at both the inlet and outlet. The exit mesh domain was extended during the meshing process to ensure that the vapor phase was zero at the outlet, regardless as to whether cavitation occurred or not during the simulation.

A transient analysis was conducted using the aforementioned model. When using the uniform geometry, the solution was initialized using ANSYS's hybrid initialization option at 15 iterations. As the simulation began, the iterations per time step were set to a value above 1500 since reaching convergence was expected to take longer with the added variable.

For the 1.5 pitch geometry, the single-phase solution was produced to determine the properties at each node within the mesh. The data obtained from the single phase solution was utilized as the initialization for the multiphase model. Importing the single phase data allowed for the multiphase solution to be solved with greater ease than if a hybrid initialization was used instead. The time step value was reduced by half, to a value of 0.006 seconds, before allowing the

simulation to commence. The solution method was set to “SIMPLEC” with a correction value set to three. With the use of “SIMPLEC”, skewness that exists within the mesh as a result of the inflation applied to the blade and fluid wall surface, is accounted for. In addition to mesh skewness, “SIMPLEC” also helps alleviate the rigidity of the model caused by the coupling of velocity and pressure [20]. The equation for “SIMPLEC” is shown in Equation 21.

$$J_f = J_f^* + d_f (p'_{c0} - p'_{c1}) \quad (21)$$

Where:

J_f is the corrected face flux,

J_f^* is the face flux,

d_f is the correction coefficient,

p'_{c0} is the pressure correction at $c0$,

p'_{c1} is the pressure correction at $c1$,

$c0$ denotes cell “0”, and

$c1$ denotes cell “1”, which is adjacent to cell “0”.

Due to the rotation existing within the fluid, “PRESTO!” was used to correct the pressure between iterations. At larger time steps, “PRESTO!” becomes unstable and causes divergence. Due to the onset of divergence as a result of using the “PRESTO!” option, the pressure correction method is set to “Linear” after approximately two to four time steps. The flow chart encompassing the simulation involving the aforementioned solution, pressure, and momentum correction methods can be seen in Figure 10.

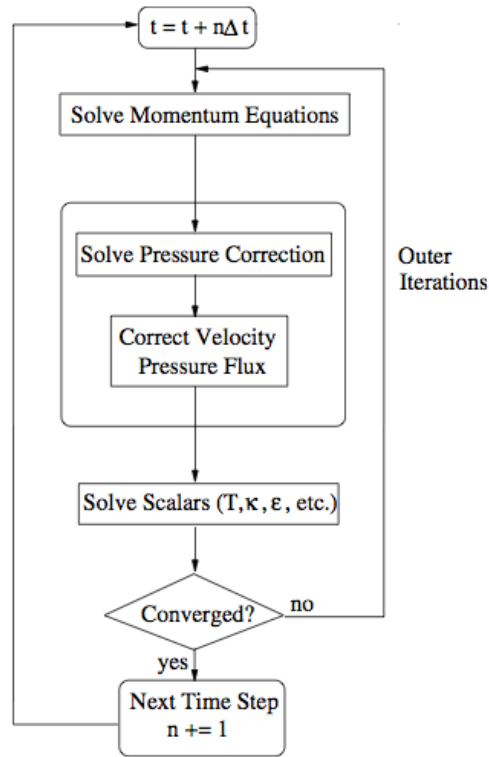


Figure 10. Flow chart for transient simulations [20].

Three important performance characteristics were determined for the turbine, the head required to produced the inlet flow rate, the power produced by the turbine, and the efficiency of the turbine. Equations 22 through 24 display the the methodology used in determine the key turbine performance characteristics.

$$h = \frac{\Delta P}{\rho g} \quad (22)$$

Where:

h is the head,

g is gravity, and

ΔP is the pressure difference between inlet and exit of the turbine.

$$W_{turb} = \tau \Omega \quad (23)$$

Where:

W_{turb} is the maximum theoretical power produced by the turbine,
 τ is the torque produced by the blade, and
 Ω is the rotation rate of the blade.

$$\eta_{turb} = \frac{\Delta P}{\rho g h} \times 100\% \quad (24)$$

Where:

η_{turb} is the efficiency of the turbine.

During post processing, the Cavitation number was utilized to determine the critical value at which the onset of cavitation occurs. By introducing the Cavitation number to the flow regime, the domain becomes non-dimensionalized in such a way to allow areas where cavitation, if it exists within the flow, is occurring regardless as to whether the simulation is single phase or multiphase. Cavitation number is the ratio of local static pressure head above the vapor pressure of the fluid to the dynamic pressure. The relationship used for Cavitation number can be seen in Equation 25 [22].

$$\sigma = \frac{P - P_v}{\frac{1}{2} \rho V_{ref}^2} \quad (25)$$

Where:

σ is the Cavitation number,

P is the local pressure,

P_v is the vapor pressure, and

V_{ref} is a referential velocity.

A secondary volume, seen in Figure 11, was created for the Cavitation number study. Due to the large number of elements that existed in the entire fluid domain, it was advantageous to create a separate volume that contained only the

blade. Through creating the secondary volume, unnecessary nodal data was eliminated which allowed for the exportation of nodal data, calculation of Cavitation number, and importation of nodal data back into FLUENT to be done faster and more efficiently.

The referential velocity within the flow is determined by averaging the velocity at all nodes within separated divisions along the flow domain. The referential velocity at each division is used along with each pressure existing at the node within that section. To determine the Cavitation number using Equation 25, the density, pressure, and velocity in the stationary frame were exported from the CFD-Post to an excel “.csv” file. The data was then inputted into a Matlab program that incorporated Equation 25 and produced a data file that included each parameter along with the corresponding cavitation number. The user then attached the line and connectivity values associated with each face of the element and the final file was imported back into CFD-Post. The source code used to determine the Cavitation number for the single phase model and multiphase model may be seen in Appendix C and Appendix D.

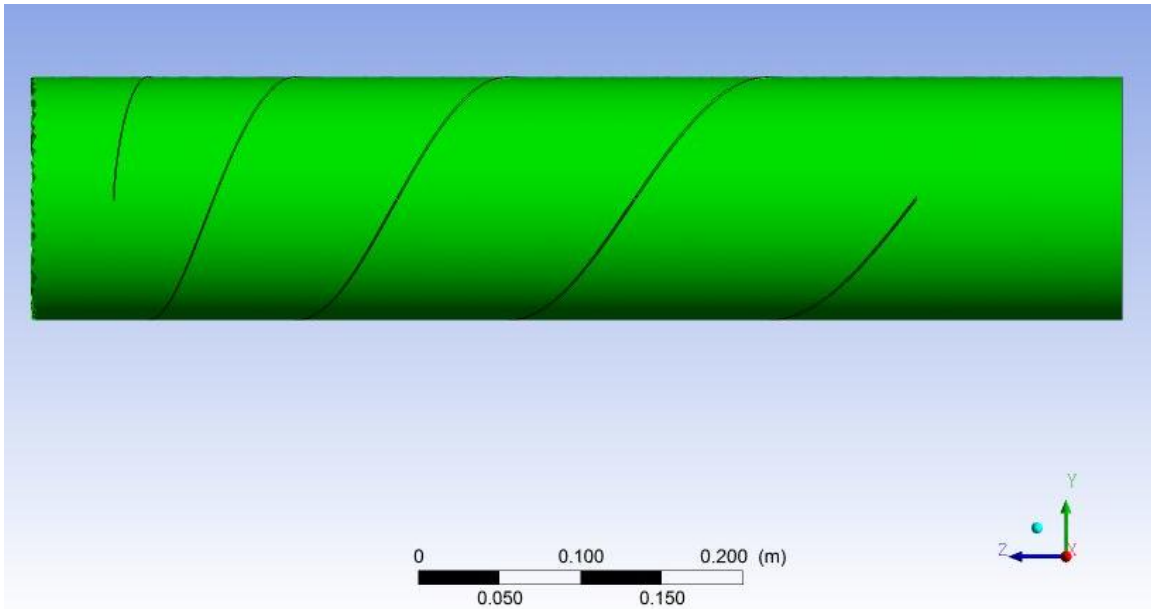


Figure 11. Secondary volume produced for Cavitation number study.

Results and Discussion

With the additional phase in the multiphase simulation, the outlet pressure required for convergence was higher than that of the single phase simulation at the same boundary conditions. Therefore, the head required for convergence was larger for the multiphase simulations than it was with the corresponding single phase simulations. Since the head was larger, the pressures associated with the flow were greater. Therefore, the multiphase model cannot be validated based purely on comparison between the pressure distribution, despite both simulations showing similar pressure contours. To ensure that the flows occurring within both simulations are almost identical, a vortex core region was used incorporating swirl intensity with a value of 676.3 s^{-1} and being color coded based on the velocity field. Figure 12 shows the pressure contours with the aforementioned swirl intensity vortex core region for both single phase and multiphase simulations. Both simulations show the same flow characteristics based on the same value of swirl intensity. The discrepancy between the two images is due to the secondary phase volume fraction that exists since cavitation is occurring. When no cavitation occurred within the flow, the pressure drop from the inlet to the outlet increased to values much larger than what could be expected and performance values did not agree with the performance values observed in the single phase simulations. The discrepancy between the two methods is caused by the additional equations implemented involving the additional phase. More specifically, model may be over constrained in the absence of a secondary phase. The multiphase model may be used to determine whether or not cavitation occurs, but does not yield usable flow

characteristics if no cavitation is present within the fluid domain; meaning that the multiphase simulation is on truly valid when a secondary phase is present within the fluid domain.

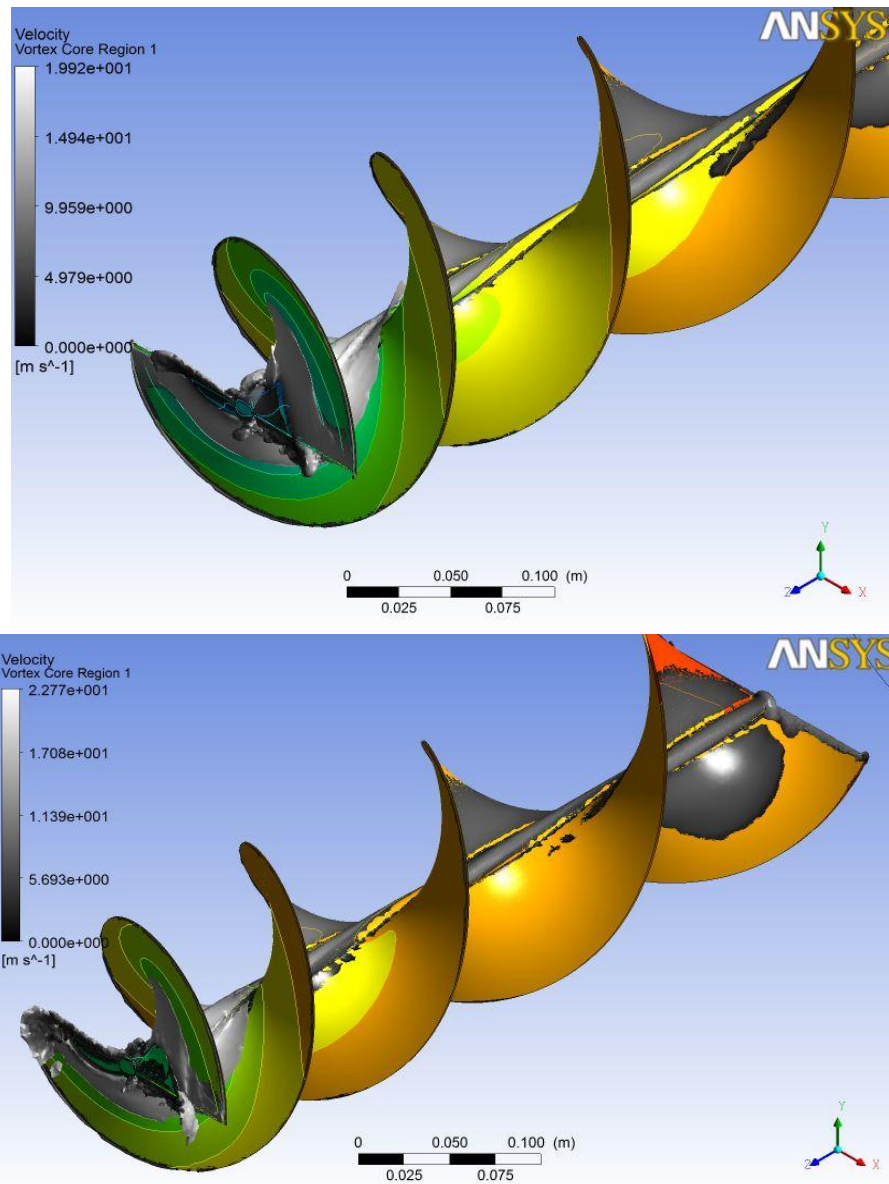


Figure 12. Pressure contour with vortex core region based on a swirl intensity of $676.3\ s^{-1}$ for multiphase flow (above) and single phase flow (below) at a flow rate of $.1\ m^3/s$ and a rotation rate of 500 rpm.

The volume fraction of the second phase along the blade for the 1.5 pitch geometry at a flow rate of $0.0625 \text{ m}^3/\text{s}$ and a rotation rate of 500 rpm can be seen in Figure 13. Only two small regions exist on the blade, one on the side shown in Figure 13 and one on the opposite side of the blade. No cavitation occurs when the inlet flow is $0.05 \text{ m}^3/\text{s}$, so the onset of cavitation at the given rotation rate occurs between the two flows. Figure 14 shows the volume fraction on the uniform pitch geometry when the inlet flow rate is $0.5 \text{ m}^3/\text{s}$ and the rotation rate is 500 rpm. For the same geometry and rotation rate, no cavitation occurred when the flow rate was $0.25 \text{ m}^3/\text{s}$. Despite a large range in flow rate where the onset of cavitation may occur, it is unnecessary to produce any additional results for the uniform geometry since it is not the ideal blade design for producing power. The purpose of determining the multiphase characteristics for flow over a uniform geometry is to determine, to what extent, the geometry has on cavitation and the onset of cavitation. The onset of cavitation for the uniform geometry occurs at flow rate approximately four to eight times the flow rate at which the onset occurs for the 1.5 pitch geometry. The onset of cavitation, therefore, is extremely dependent of blade geometry; but more specifically, the pitch angle of the blade. For the 1.5 pitch geometry, Figure 15 shows the how the secondary phase developing on the blade as velocity increased. As the flow rate at the inlet increases, the cavitation that occurs at the turbine exit intensifies. As the cavitation intensifies, addition vortex shedding occurs and produces addition regions of cavitation beyond the blade. Figure 16 shows where the volume fraction as it develops off of the blade as well as the regions that it exists within the swirling flows.

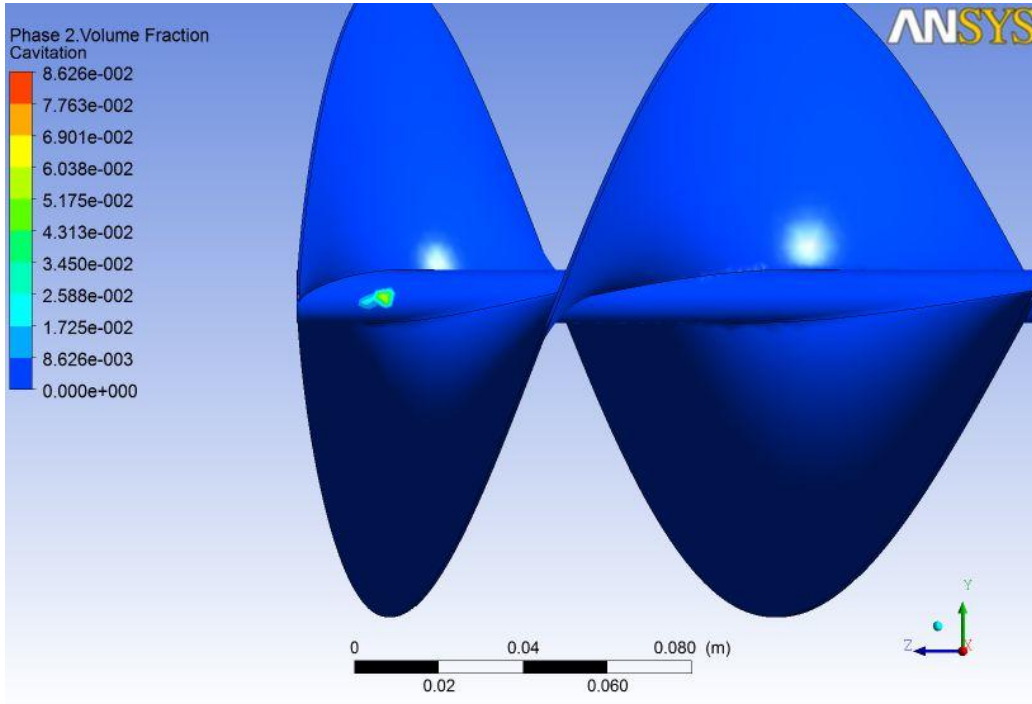


Figure 13. Vapor fraction along blade on 1.5 pitch geometry with flow rate of $0.0625 \text{ m}^3/\text{s}$ and a rotation rate of 500 rpm.

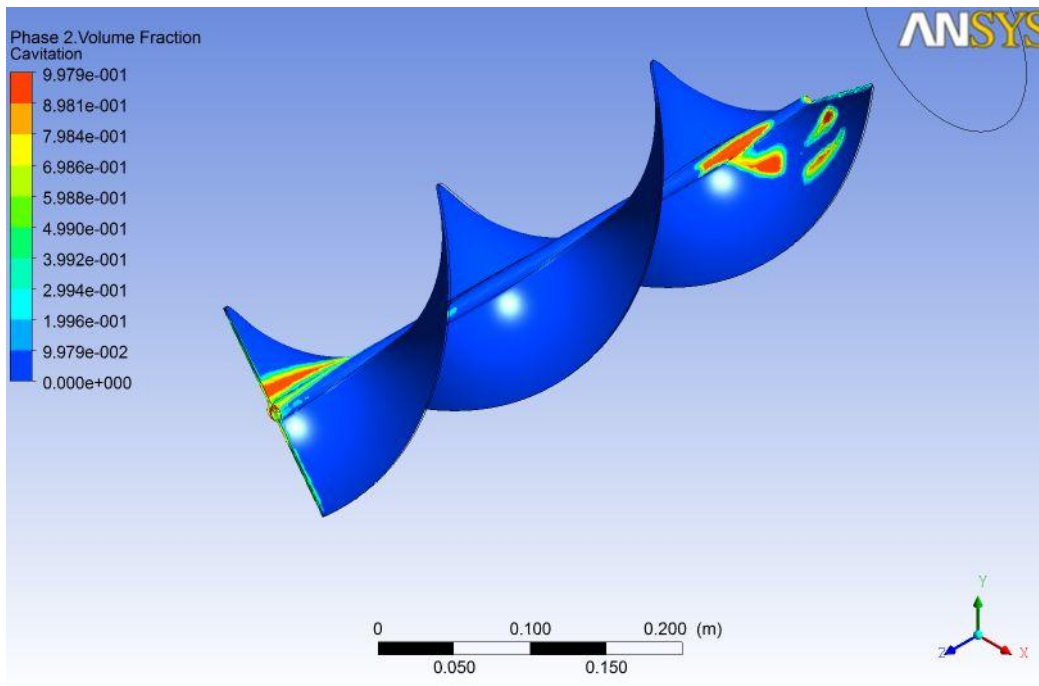


Figure 14. Vapor fraction along blade on uniform geometry with flow rate of $0.5 \text{ m}^3/\text{s}$ and a rotation rate of 500 rpm.

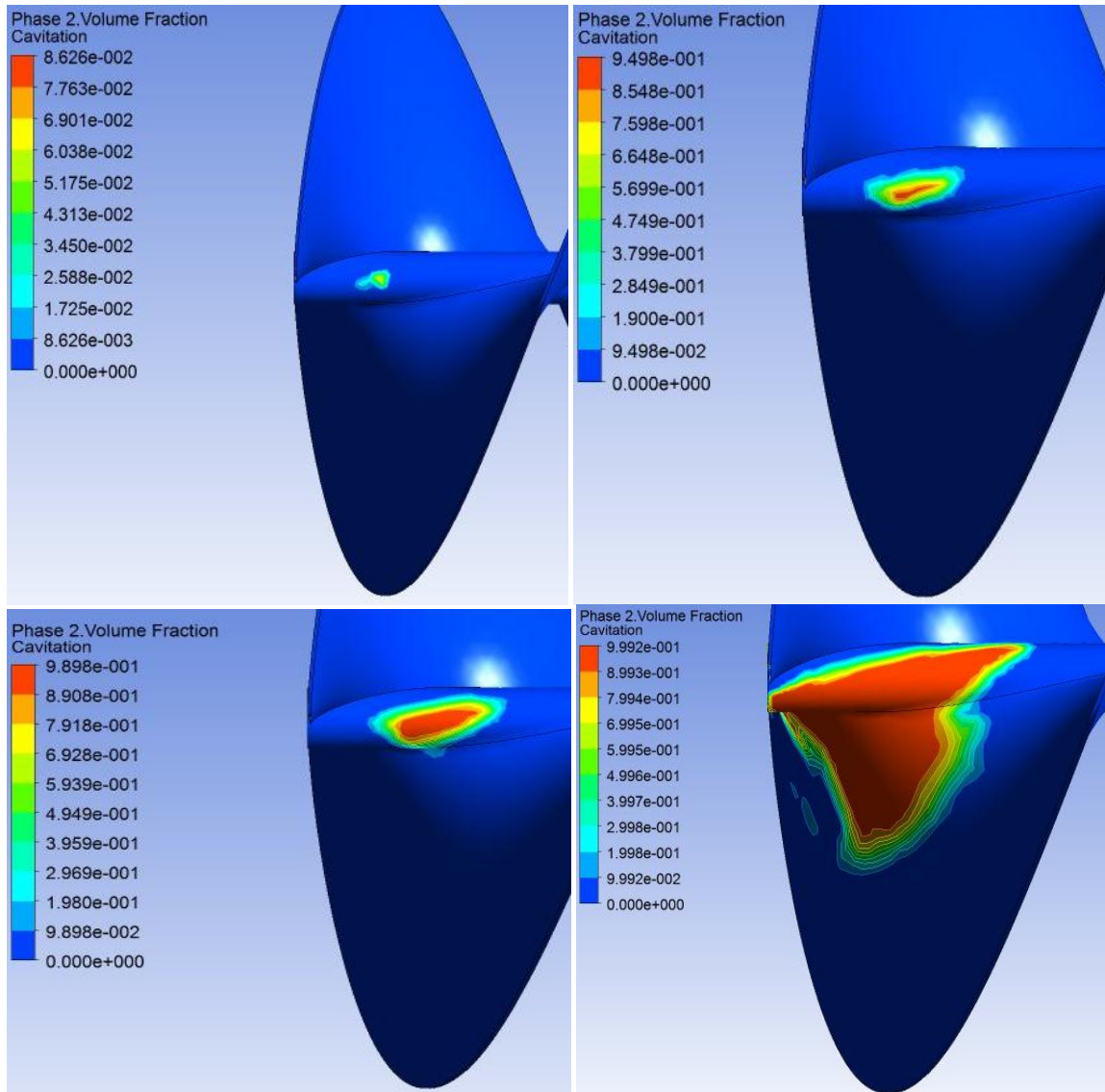


Figure 15. Cavitation on blade of 1.5 pitch geometry operating at a rotation rate of 500 rpm for flow rates of 0.0625 m³/s (top left), 0.075 m³/s (top right), 0.0875 m³/s (bottom left), and 0.1 m³/s (bottom right).

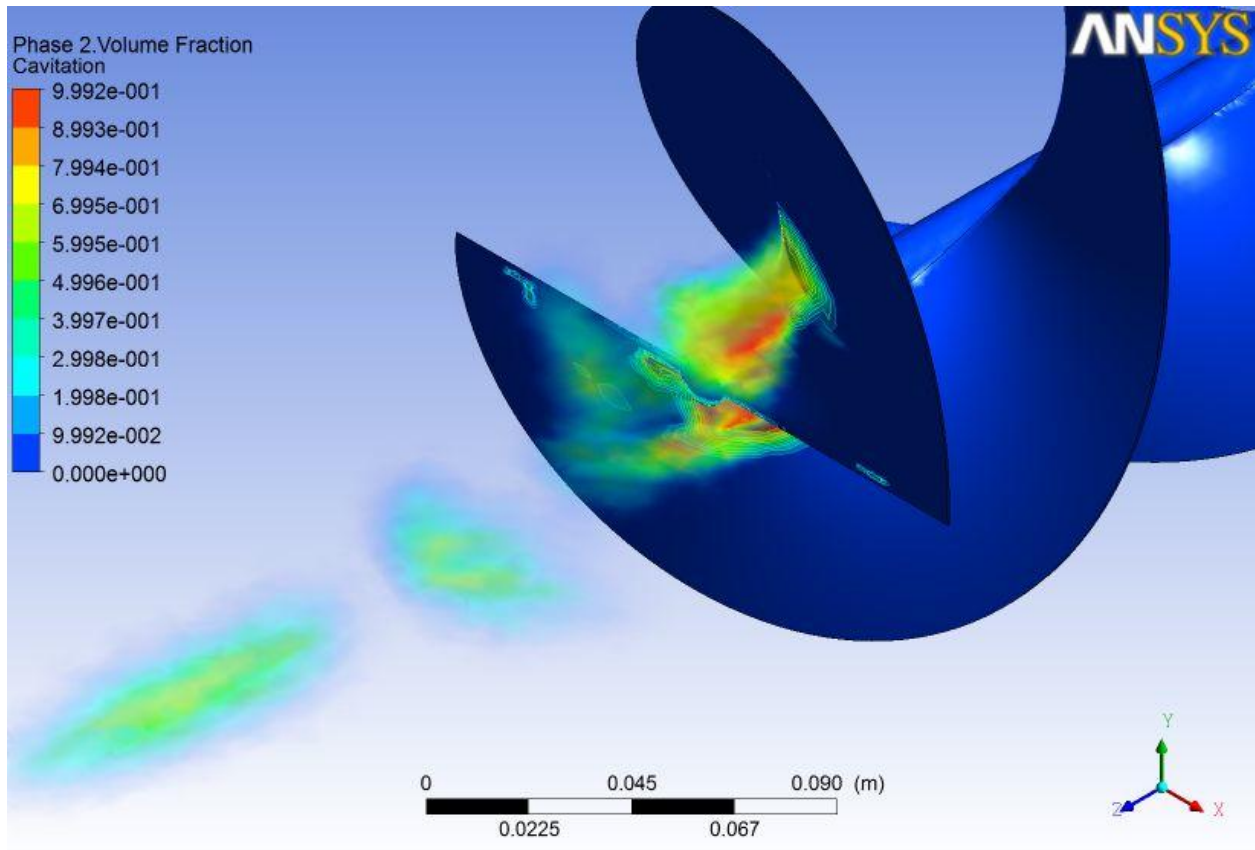


Figure 16. Volume fraction exiting the turbine for the 1.5 pitch geometry at a flow of $0.1 \text{ m}^3/\text{s}$ and a rotation rate of 500 rpm.

Figure 17 shows the relationship between head required for convergence and flow rate using the 1.5 pitch geometry. In the multiphase simulations, as flow rate increased past the point in which the onset of cavitation occurs, the head required for convergence increases at a much faster rate than the head values required for the single phase solution to converge. Similarly to Figure 17, Figure 18 shows the power produced, for the same 1.5 pitch blade turbine, as a function of flow rate. The power increases at a faster rate in the multiphase simulations than that of the single phase simulations as velocity increase past the cavitation onset flow rate. Finally, in Figure 19, the relationship between efficiency and flow rate can be seen for both multiphase flow and single phase flow. At the onset of cavitation,

the drop in efficiency was only approximately one percent. As the vapor phase increased at the exit of the turbine, the efficiency drop between single phase and multiphase simulations ranged from 8% to 12%. All performance data obtained from the simulations can be found in Appendix E.

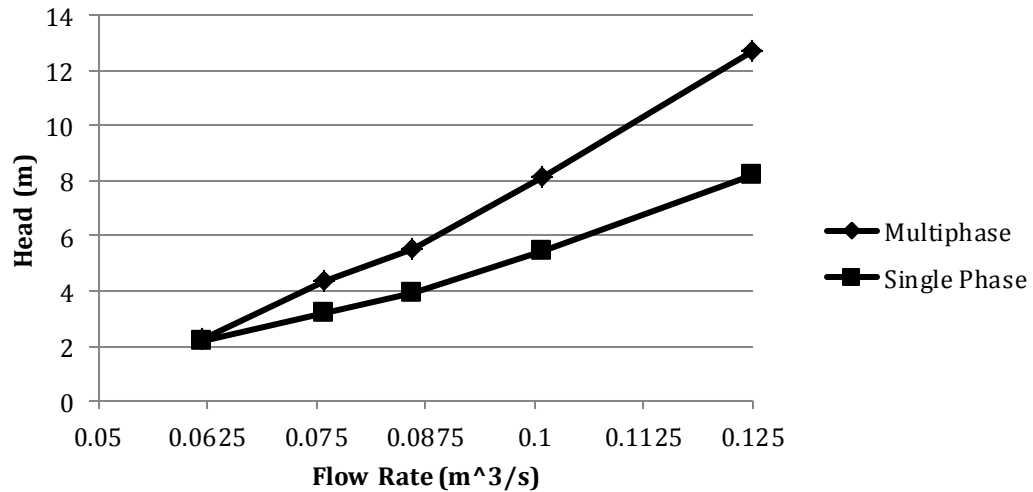


Figure 17. Head as a function of flow rate for multiphase and single phase models simulations with the 1.5 pitch geometry and rotation rate of 500 rpm.

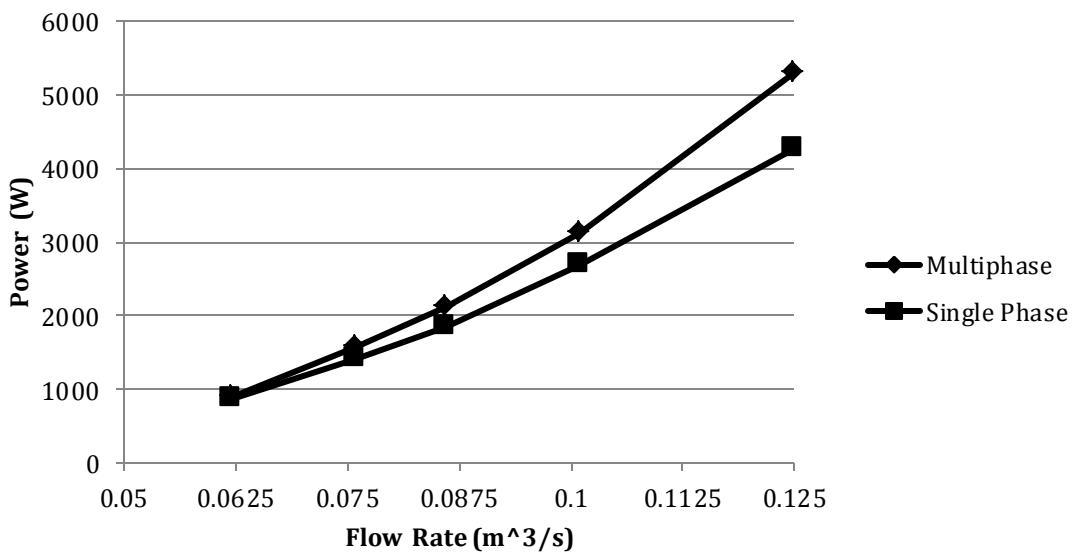


Figure 18. Power as a function of flow rate for multiphase and single phase simulations with the 1.5 pitch geometry and rotation rate of 500 rpm.

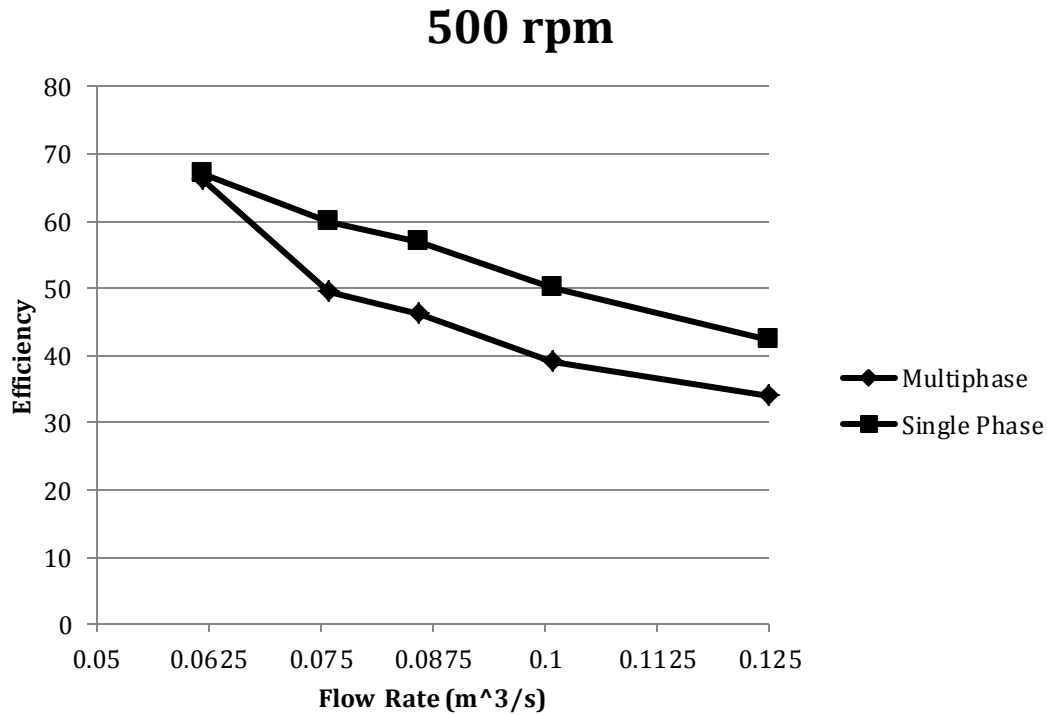


Figure 19. Efficiency as a function of flow rate for both multiphase and single phase simulations with the 1.5 pitch geometry and rotation rate of 500 rpm.

Figure 20 shows the Cavitation number and volume fraction along the blade within the multiphase simulation with a flow rate of 0.1 m³/s. As seen in Figure 20, Cavitation number contours and the volume fraction contours match almost perfectly. From Figure 20, it is determined that the critical Cavitation number, which the onset of cavitation will occur, lies within the range of -30,000 to -20,000. Applying the critical Cavitation number based on the multiphase simulation to the single phase simulation, the Cavitation number contour produced is shown in Figure 21. A few discrepancies exist between the Cavitation number observed in Figure 20 compared to those observed in Figure 21. The single phase simulation does not have volume fraction present within the flow regime to influence the various variables such as pressure, velocity, and density within the flow. Therefore, the

single phase model will not exhibit results that align perfectly with those of the multiphase model. The shape of the contours within the single phase simulation are almost identical to that seen in multiphase simulation, however the contours are all rotated about the z-axis along the blade and shaft. Additionally, the flow rate used for the comparison is an extreme case. Figure 22 compares the Cavitation number and volume fraction for the multiphase simulation with a flow rate of $0.0625 \text{ m}^3/\text{s}$. Figure 23 shows the Cavitation for the single phase simulation with the same boundary conditions. Figure 22 and Figure 23 show the similarities between the Cavitation number produced shortly after the onset of cavitation occurs. In Figure 22 it can be seen that the Cavitation number aligns almost exactly with the volume contours along the blade, similarly to Figure 20. The Cavitation numbers produced by single phase and multiphase simulations for a flow rate of $0.0625 \text{ m}^3/\text{s}$ differ slightly in the minimum Cavitation number (indication the intensity of cavitation) produced, but otherwise show the same region where cavitation is most likely. Accuracy in using the Cavitation number improves the closer the flow rate is to the flow rate at which cavitation occurs.

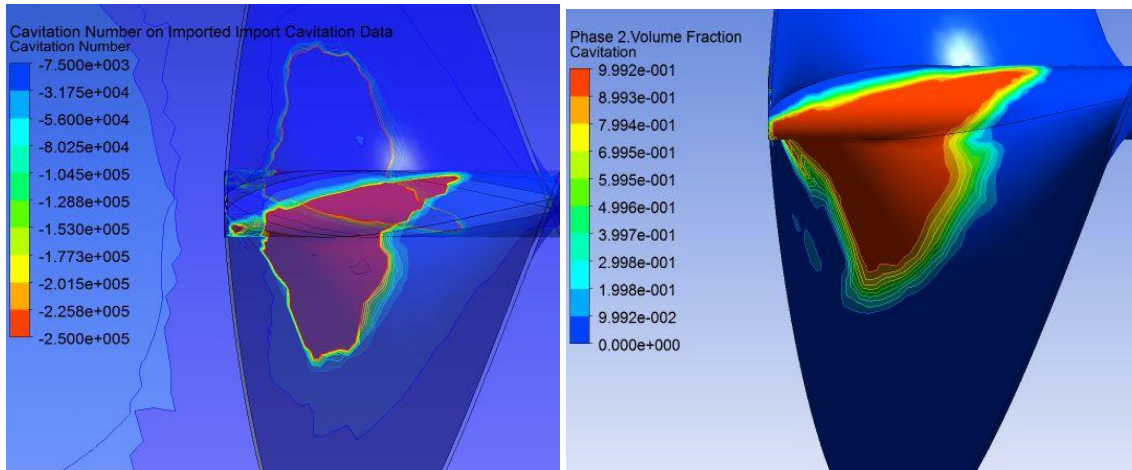


Figure 20. Cavitation number (left) and volume fraction (right) contours along the blade for the multiphase simulation with flow rate of $0.1 \text{ m}^3/\text{s}$.

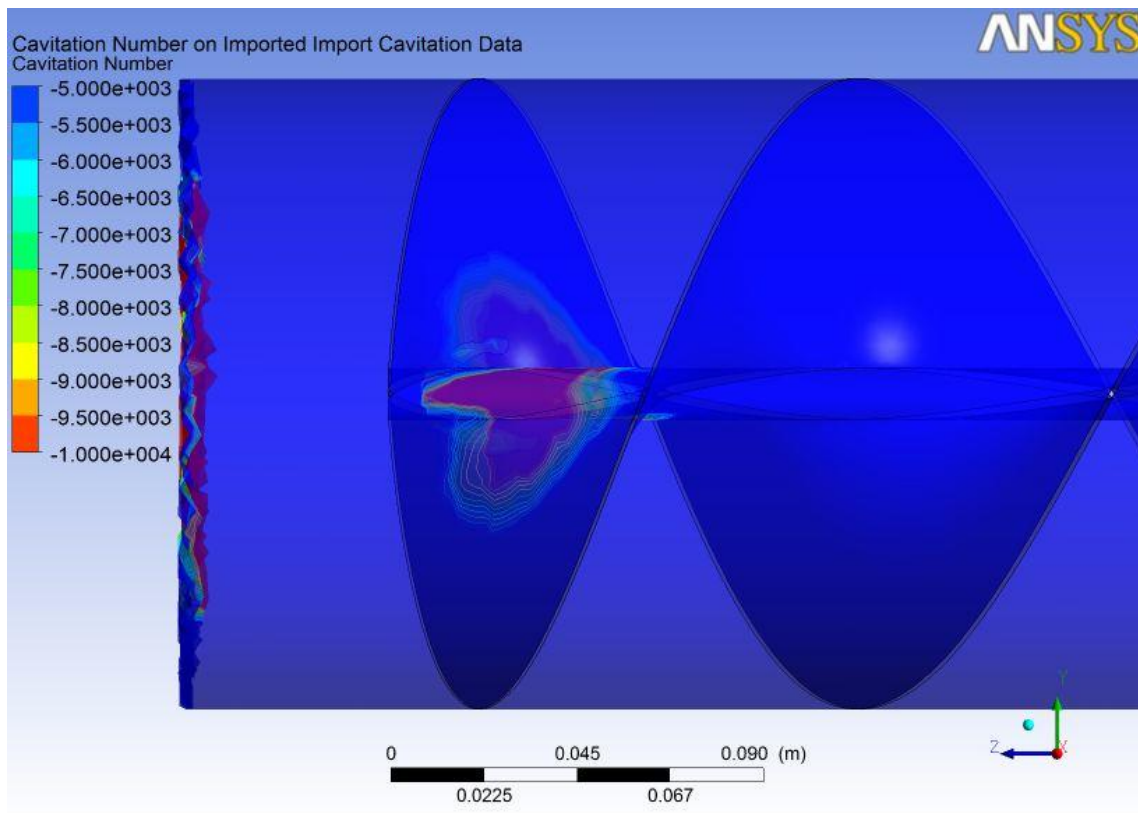


Figure 21. Cavitation number along blade for single phase simulation with flow rate of $0.1 \text{ m}^3/\text{s}$.

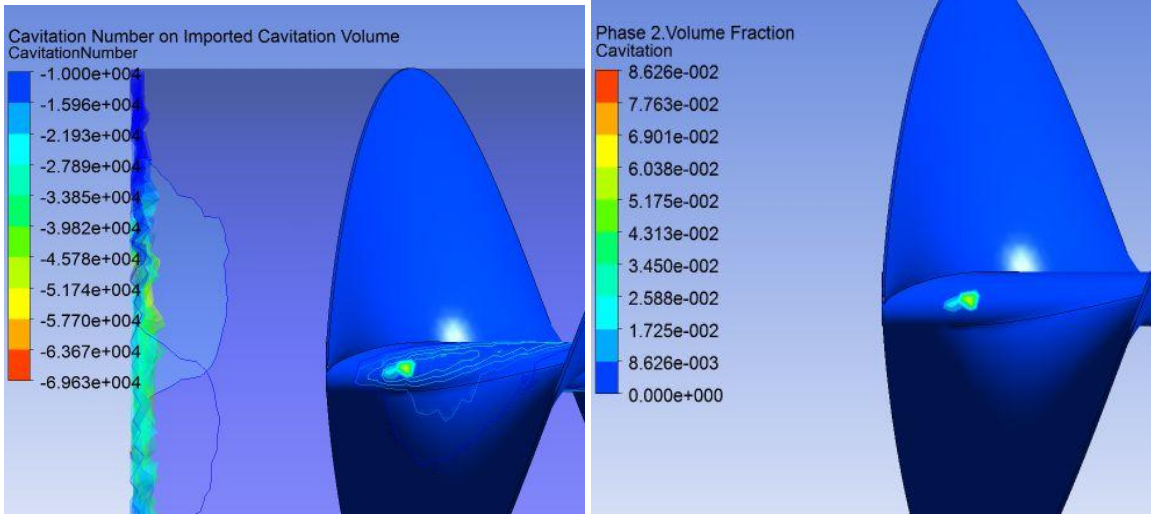


Figure 22. Cavitation number (left) and volume fraction (right) contours along the blade for the multiphase simulation with flow rate of $0.0625 \text{ m}^3/\text{s}$.

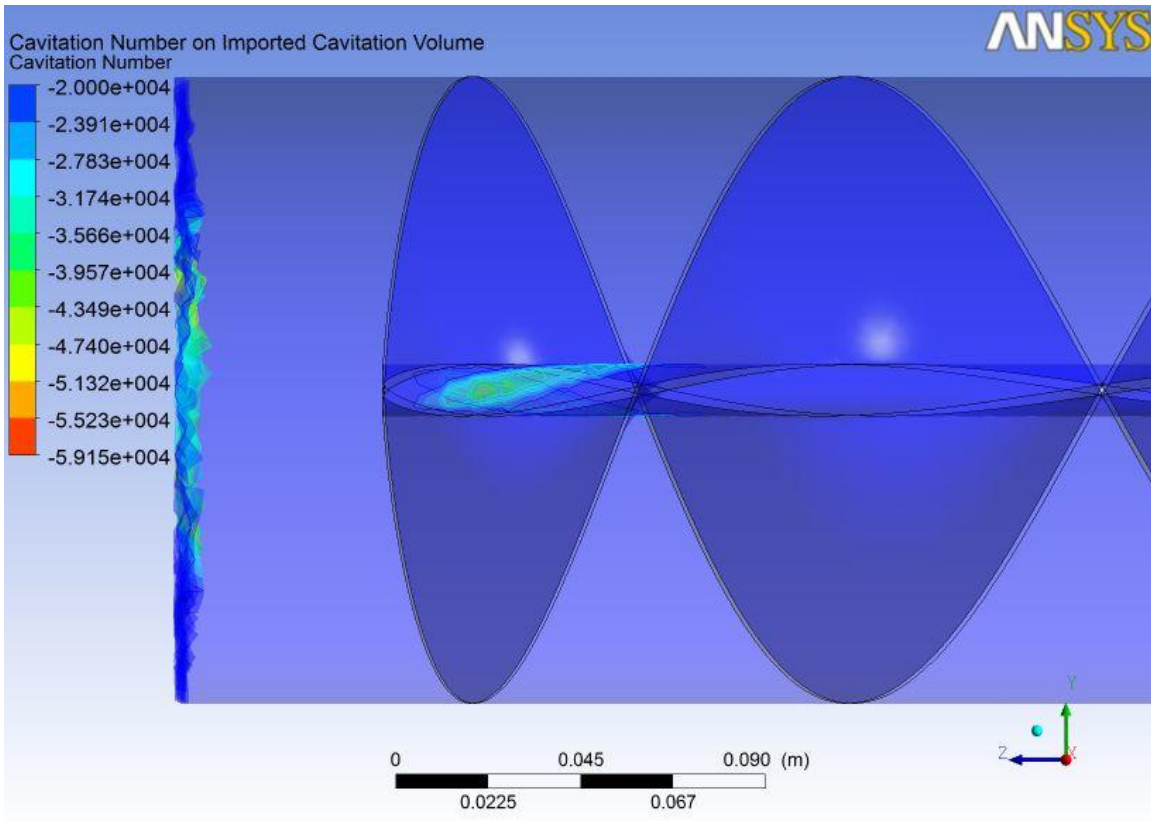


Figure 23. Cavitation number along blade for single phase simulation with flow rate of $0.0625 \text{ m}^3/\text{s}$.

Conclusions

The multiphase model provides accurate results of regions where cavitation is expected to occur. Through the use of the vortex core regions, the multiphase model can be validated as both multiphase and single phase simulations show almost identical results based on the swirl intensity and the velocity field. The cavitation model can be used to determine if cavitation occurs; however, if no cavitation is present, the performance characteristics that are produced by the simulation are not accurate.

The uniform geometry is a more robust design that allows for a much larger flow rate to be used than the 1.5 pitch geometry before cavitation occurs. For the 1.5 pitch geometry, the onset of cavitation occurs between the flow rates of 0.05 m³/s and 0.0625 m³/s. The uniform geometry doesn't show signs of cavitation until flows beyond 0.25 m³/s. Using the uniform geometry is not ideal since the 1.5 pitch geometry produces approximately two to three times as much power at the same flow rate. Therefore, to maximize the power produced by the turbine while increasing the flow rate where the onset of cavitation occurs, the pitch of the blade must be altered accordingly. The power increased for the multiphase simulations as did the head required for the solution to converge. As a result of the power and head trends, efficiency dropped as flow rate exceeded the flow rate at which the onset of cavitation occurred. As the intensity of cavitation increases, efficiency drops of approximately 12% are observed.

Finally, the use of Cavitation number allows for the single phase solution to be used directly in order to determine if cavitation is likely to occur. Using the Cavitation number within the single phase solution does not allow for the turbine performance characteristics of the multiphase solution to be determined, such as torque, power, and efficiency, to be determined. Despite not being able to produce key characteristics exhibited by the flow and the geometry, the Cavitation number is useful in determining the onset of cavitation and predicting regions that contain a high volume fraction within the flow without the use of long simulations that require the allocation of many computational resources.

References

- [1] "How a microhydropower system works" U.S. Department of Energy. [Online]. Available: <http://energy.gov/energysaver/articles/microhydro-systems> [accessed 12 September 2012]
- [2] Idaho National Laboratory, "Virtual Hydropower Prospector," 24 May 2011. [Online]. Available: <http://hydropower.inel.gov/prospector/index.shtml>. [Accessed 12 September 2012].
- [3] M. R. Nouni, S. C. Mullick and T. C. Kandpal, "Techno-economics of micro-hydro projects for decentralized power supply in India," *Energy Policy*, vol. 34, no. 10, p. 1161–1174, 2006.
- [4] O. Paish, "Small hydro power: technology and current status," *Renewable and Sustainable Energy Reviews*, p. 537–556, 2002.
- [5] Alexander, K.V., Giddens, E.P., and Fuller, A.M., "Radial- and mixed-flow turbines for low head microhydro systems," *Renewable Energy*, vol. 34, n 7, p 1885-1894, July 2009.
- [6] Alexander, K.V., Giddens, E.P., "Optimum penstocks for low head microhydro schemes," *Renewable Energy*, vol. 33, n 3, p 507-519, 2008.
- [7] Alexander, K.V., Giddens, E.P., "Microhydro: Cost-effective, modular systems for low heads," *Renewable Energy*, vol. 33, n 3, p 1379-1391, 2008.
- [8] Alexander, K.V., Giddens, E.P., and Fuller, A.M., "Axial-flow turbines for low head microhydro systems," *Renewable Energy*, vol. 34, p 35-47, July 2008.
- [9] Singh, P., Nestmann, F., "Experimental investigation of the influence of blade height and blade number on the performance of low head axial flow turbines," *Renewable Energy*, vol. 36, p 272-281, 2011.
- [10] Ding, H., Visser, F. C., Jiang, Y., and Furmanczyk, M., "Demonstrating and Validation of a 3D CFD Simulation Tool Predicting Pump Performance and [3]Cavitation for Industrial Applications," *Journal of Fluids Engineering, Transactions of the ASME*, vol. 133, n 1, 2011.
- [11] Srinivasan, V., Salazar, A., and Saito, K., "Numerical simulation of cavitation dynamics using a cavitation-induced-momentum-defect (CIMD) correction approach," *Applied Mathematical Modeling*, vol. 33, p 1529-1559, 2009.
- [12] Singhal, A., Athavale, M., Li, H., and Jiang, Y., "Mathematical Basis and Validation of the Full Cavitation Model," *Journal of Fluids Engineering*, vol. 124, p 617-624, September 2002.

- [13] Medvitz, R., Kunz, R., Boger, D., and Lindau, J., "Performance Analysis of Cavitating Flow in Centrifugal Pumps Using Multiphase CFD," *Journal of Fluids Engineering*, vol. 124, p 377-, June 2002.
- [14] Shukla, S. and Kshirsagar, J., "Numerical Prediction of Cavitation in Model Pump," *2008 ASME International Mechanical Engineering Congress and Exposition*, p 91-98. [4]
- [15] Li, H., Kelecý, F., Egelja-Maruszewski, A., and Vasquez, S., "Advanced Computational Modeling of Steady and Unsteady Cavitating Flows," *2008 ASME International Mechanical Engineering Congress and Exposition*, p 413-423.
- [16] Escaler, X., Egusquiza, E., Farhat, M., Avellan, F., and Coussirat, M., "Detection of cavitation in hydraulic turbines," *Mechanical Systems and Signal Processing*, vol. 20, p 083-1007, 2006.
- [17] Schleicher, W.C., Ma, H., Riglin, J., Wang, C., Kraybil, Z., Wei, W., Klein, R., and Oztekin, A., "Characteristics of a Micro Hydro Turbine" *Computers and Fluids*, Under Review
- [18] V. Yakhot and S. A. Orszag, "Renormalization-Group Analysis of Turbulence," *Applied and Computational Mathematics*, vol. 57, no. 14, pp. 1722-1724, 6 October 1986.
- [19] V. Yakhot, S. A. Orszag, S. Thangam, T. B. Gatski and C. G. Speziale, "Development of turbulence models for shear flows by a double expansion technique," *American Institute of Physics*, vol. 4, no. 7, pp. 1510-1520, July 1992.
- [20] ANSYS, Inc., "Theory Guide," 2009.
- [21] ANSYS, Inc., "ANSYS 12.0 User's Guide," 2009.
- [22] d'Agostino, Salvetti, M., "Fluid Dynamics of Cavitation and Cavitating Turbopumps", Springer, 2008, pp. 1-15.

Appendices

Appendix A: 2.5 turn, uniform pitch dimensioned drawing

Appendix B: 2.5 turn, 1.5 pitch dimensioned drawing

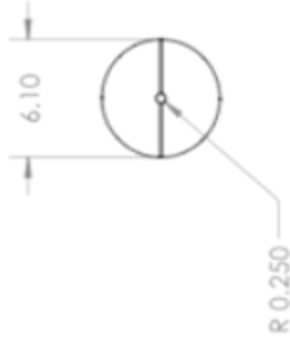
Appendix C: Cavitation number source code for single phase simulation

Appendix D: Cavitation number source code for multiphase simulation

Appendix E. Data Tables

Appendix A: 2.5 turn, uniform pitch dimensioned drawing

CONSTANT PITCH
2.5 TURNS



UNLESS OTHERWISE SPECIFIED:		NAME	DATE
DIMENSIONS ARE IN INCHES		ZK	
TOLERANCES:			
FRACTIONAL 1	BEND 1		
ANGULAR MATCH	TWO PLACE DECIMAL		
THREE PLACE DECIMAL			
INTERPRET GEOMETRIC TOLERANCING PER	COMMENTS:		
MATERIAL			
FINISH			
NEST ASST	USED ON		
APPLICATION	DO NOT SCALE DRAWING		

TITLE: 2.5 TURNS
CONSTANT PITCH

SIZE DWG. NO. REV
A

SCALE: 1:8 WEIGHT: SHEET 1 OF 1

5
PROPRIETARY AND CONFIDENTIAL
 THE INFORMATION CONTAINED IN THIS DRAWING IS THE SOLE PROPERTY OF <INSERT COMPANY NAME HERE>. ANY REPRODUCTION IN PART OR AS A WHOLE WITHOUT THE WRITTEN PERMISSION OF <INSERT COMPANY NAME HERE> IS PROHIBITED.

1 2 3 4

Appendix B: 2.5 turn, 1.5 pitch dimensioned drawing

**POWER 1.5 PITCH
2.5 TURNS**



UNLESS OTHERWISE SPECIFIED:		NAME	DATE	TITLE:	
DIMENSIONS ARE IN INCHES		ZK		POWER 1.5 PITCH	
TOLERANCES				2.5 TURNS	
FRACTIONS 1				SIZE	REV
ANGULAR MATCH BEND 1				A	
TWO PLACE DECIMAL 2				SCALE: 1:16 WEIGHT:	SHEET 1 OF 1
THREE PLACE DECIMAL 3					
INTERPRET GEOMETRIC TOLERANCING PER MATERIAL					
G.A.					
COMMENTS:					
NEXT ASSY USED ON					
APPLICATION					
DO NOT SCALE DRAWING					

PROPRIETARY AND CONFIDENTIAL
 THE INFORMATION CONTAINED IN THIS DRAWING IS THE SOLE PROPERTY OF <INSERT COMPANY NAME HERE>. ANY REPRODUCTION IN PART OR AS A WHOLE WITHOUT THE WRITTEN PERMISSION OF <INSERT COMPANY NAME HERE> IS PROHIBITED.

Appendix C: Cavitation number source code for single phase simulation

```
% Jacob Riglin
% 1.5 Pitch Geometry, 500rpm rotation rate, .1m3/s flow rate

%-----%
%-----%
% This program converts imported data from CFD-Post, produces a
cavitation
% number, and utilizes a final matrix that can be imported back
into
% FLUENT.
% File designed for singlephase simulation
%-----%
%-----%
clear
clc

% Parameters
P_v=3540; % Vapor pressure [Pa]

% Import multiphase data (Option 1:.csv file; Option 2:.txt file)
M=xlsread('singlephase_.1m3s_500rpm.csv');
% M = importdata('multiphase_.1m3s_500rpm.txt');

%%
% Notes on M
% Column 1: Nodes []
% Column 2: X position [m]
% Column 3: Y position [m]
% Column 4: Z position [m]
% Column 5: Density [kg m^-3]
% Column 6: Pressure [Pa]
% Column 7: Velocity in Stn Frame [m s^-1]

n=80; % Divisions along length
L=max(M(:,4)-min(M(:,4))); % Max length [m]
deltaL=L/n; % length interval [m]

l_int=min(M(:,4)); % Initial L step
for i=1:n;
    vel=0; % Velocity vector
    for j=1:length(M(:,4))
        if (M(j,4)<(l_int+deltaL)) && (M(j,4)>(l_int))
            vel(j)=M(j,7);
        end
    end
    % Determine refernce velocity
    v_ref(i)=mean(vel);
    % Determine cavitation number
    for j=1:length(M(:,4))
        if (M(j,4)<=(l_int+deltaL)) && (M(j,4)>=(l_int))
            % Cavitation number; Row1-Corresponding Node, Row2-Cav.
            Number
```

```

sigma_c(j,1)=(M(j,1));
cn=(M(j,6)-P_v)/(0.5*M(j,5)*v_ref(i)^2); % Cavitation number
if -1e15<cn&&cn<1e15 % Provide cutoff for cavitation number
sigma_c(j,2)=cn;
elseif cn<=-1e15
    sigma_c(j,2)=-1e15;
else
    sigma_c(j,2)=1e15;
end
end
end
end
l_int=l_int+deltaL; % Updated L step
end

% Column 9 of M becomes Cavitation number
M(:,8)=sigma_c(:,2);
%%
save cavdata1.xls M -ascii

```

Appendix D: Cavitation number source code for multiphase simulation

```
% Jacob Riglin
% 1.5 Pitch Geometry, 500rpm rotation rate, .1m3/s flow rate

%-----%
% This program converts imported data from CFD-Post, produces a
cavitation
% number, and utilizes a final matrix that can be imported back
into
% FLUENT.
% File designed for multiphase simulation
%-----%
clear
clc

% Parameters
P_v=3540; % Vapor pressure [Pa]

% Import multiphase data (Option 1:.csv file; Option 2:.txt file)
M=xlsread('multiphase_.1m3s_500rpm.csv');
% M = importdata('multiphase_.1m3s_500rpm.txt');

%%
% Notes on M
% Column 1: Nodes []
% Column 2: X position [m]
% Column 3: Y position [m]
% Column 4: Z position [m]
% Column 5: Density [kg m^-3]
% Column 6: Phase 2 Volume Fraction []
% Column 7: Pressure [Pa]
% Column 8: Velocity in Stn Frame [m s^-1]

n=80; % Divisions along length
L=max(M(:,4)-min(M(:,4))); % Max length [m]
deltaL=L/n; % length interval [m]

l_int=min(M(:,4)); % Initial L step
for i=1:n;
    vel=0; % Velocity vector
    for j=1:length(M(:,4))
        if (M(j,4)<(l_int+deltaL)) && (M(j,4)>(l_int))
            vel(j)=M(j,8);
        end
    end
    % Determine refernce velocity
    v_ref(i)=mean(vel);
    % Determine cavitation number
    for j=1:length(M(:,4))
        if (M(j,4)<=(l_int+deltaL)) && (M(j,4)>=(l_int))
```

```

                % Cavitation number; Row1-Corresponding Node, Row2-Cav.
Number
    sigma_c(j,1)=(M(j,1));
    cn=(M(j,7)-P_v)/(.5*M(j,5)*v_ref(i)^2); % Cavitation number
    if -1e15<cn&&cn<1e15 % Provide cutoff for cavitation number
        sigma_c(j,2)=cn;
    elseif cn<=-1e15
        sigma_c(j,2)=-1e15;
    else
        sigma_c(j,2)=1e15;
    end
    end
    end
    l_int=l_int+deltaL; % Updated L step
end

% Column 9 of M becomes Cavitation number
M(:,9)=sigma_c(:,2);
%%
save cavdata.xls M -ascii
%%
scatter(sigma_c(:,2),M(:,6),'.')
xlabel('Cavitation Number'),ylabel('Phase 2 Volume Fraction')
axis([-1.5e6 1e6 0 1])

```

Appendix E. Data Tables

Table E1. Data for 1.5 pitch geometry, rotation rate of 500 rpm, multiphase

Variable	Units					
Head	[m]	12.715	8.117	5.488	4.329	2.232
Flow	[m ³ /s]	0.125	0.101	0.086	0.076	0.062
Torque	[J]	100.97	59.53	40.56	30.27	17.02
Power	[W]	5286.82	3116.96	2123.73	1585.08	891.13
Efficiency	Unitless	33.85	38.98	46.17	49.48	66.017

Table E2. Data for 1.5 pitch geometry, rotation rate of 500 rpm, single phase

Variable	Units					
Head	[m]	8.216	5.455	3.898	3.171	2.181
Flow	[m ³ /s]	0.125	0.101	0.086	0.076	0.062
Torque	[J]	81.74	51.36	35.5	26.87	16.89
Power	[W]	4279.99	2689.04	1858.69	1406.87	884.12
Efficiency	Unitless	42.409	50.06	56.93	59.98	67.01

Table E3. Data for uniform geometry, rotation rate of 500 rpm

Head	[m]	1.989	6.831	56.529	0.958	3.619	42.49
Flow	[m ³ /s]	0.1	0.15	0.5	0.1	0.15	0.5
Torque	[J]	5.082	17.679	140.184	2.2	18.366	246.504
Power	[W]	226.09	925.67	7339.99	115.19	961.63	12906.9
Efficiency	None	13.3	8.33	2.65	12.2	17.12	6.204
Phase	None	Multi	Multi	Multi	Single	Single	Single
Geometry	None	Uniform	Uniform	Uniform	Uniform	Uniform	Uniform

Vita

Jacob Daniel Riglin was born in Clearfield, Pennsylvania on December 30, 1988, to Pam and James B. Riglin II. After completing his work at Clearfield Area High School in Clearfield, Pennsylvania, he attended Bucknell University in Lewisburg, Pennsylvania. In May of 2011 he completed a Bachelor of Science in Mechanical Engineering. In August of the same year he enrolled in the Mechanical Engineering & Mechanics graduate program at Lehigh University in Bethlehem, Pennsylvania.

Permanent Address:

1208 Lumadue Street

Clearfield, PA 16830

This thesis was typed by the author.